NeuroImage: Clinical 22 (2019) 101720

Contents lists available at ScienceDirect

NeuroImage: Clinical

journal homepage: www.elsevier.com/locate/ynicl

Cerebellar resting-state functional connectivity in Parkinson's disease and multiple system atrophy: Characterization of abnormalities and potential for differential diagnosis at the single-patient level

Hugo C. Baggio[a,1], Alexandra Abos[a,1], Barbara Segura[a], Anna Campabadal[a], Carme Uribe[a], Darly M. Giraldo[b,c], Alexandra Perez-Soriano[b,c], Esteban Muñoz[b,c], Yaroslau Compta[b,c,d], Carme Junque[a,b,d], Maria Jose Marti[b,c,d,*]

[a] Medical Psychology Unit, Department of Medicine, Institute of Neuroscience, University of Barcelona, Barcelona, Catalonia, Spain
[b] Centro de Investigación Biomédica en Red sobre Enfermedades Neurodegenerativas (CIBERNED), Hospital Clínic de Barcelona, Barcelona, Catalonia, Spain
[c] Movement Disorders Unit, Neurology Service, Hospital Clínic de Barcelona, Institute of Neuroscience, University of Barcelona, Barcelona, Catalonia, Spain
[d] Institute of Biomedical Research August Pi i Sunyer (IDIBAPS), Barcelona, Catalonia, Spain

ARTICLE INFO

Keywords:
Machine learning
Parkinson's disease
Multiple system atrophy
Functional connectivity
Resting state
Cerebellum

ABSTRACT

Background: Recent studies using resting-state functional connectivity and machine-learning to distinguish patients with neurodegenerative diseases from other groups of subjects show promising results. This approach has not been tested to discriminate between Parkinson's disease (PD) and multiple system atrophy (MSA) patients.
Objectives: Our first aim is to characterize possible abnormalities in resting-state functional connectivity between the cerebellum and a set of intrinsic-connectivity brain networks and between the cerebellum and different regions of the striatum in PD and MSA. The second objective of this study is to assess the potential of cerebellar connectivity measures to distinguish between PD and MSA patients at the single-patient level.
Methods: Fifty-nine healthy controls, 62 PD patients, and 30 MSA patients underwent resting-state functional MRI with a 3T scanner. Independent component analysis and dual regression were used to define seven resting-state networks of interest. To assess striatal connectivity, a seed-to-voxel approach was used after dividing the striatum into six regions bilaterally. Measures of cerebellar-brain network and cerebellar-striatal connectivity were then used as features in a support vector machine to discriminate between PD and MSA patients.
Results: MSA patients displayed reduced cerebellar connectivity with different brain networks and with the striatum compared with PD patients and with controls. The classification procedure achieved an overall accuracy of 77.17% with 83.33% of the MSA subjects and 74.19% of the PD patients correctly classified.
Conclusion: Our findings suggest that measures of cerebellar functional connectivity have the potential to distinguish between PD and MSA patients.

1. Introduction

Parkinson's disease (PD) and multiple system atrophy (MSA) are two neurodegenerative diseases that can have overlapping clinical manifestations. Especially in early disease stages, differential diagnosis can therefore be difficult. Postmortem studies show that around 15–38% of patients with a clinical diagnosis of MSA may be incorrectly diagnosed (Koga et al., 2015; Hughes et al., 2002), with PD being the actual disease process in around 16% of misdiagnoses (Koga et al., 2015). A diagnosis of PD, on the other hand, may be shown by neuropathological examination to be mistaken in up to 35% of cases, with MSA being one of the main actual underlying disease processes (Schrag et al., 2002; Hughes et al., 1992; Litvan et al., 1998). An accurate distinction between PD and MSA is clinically relevant considering its therapeutic and prognostic implications.

Recent studies have investigated the potential of different MRI

* Corresponding author at: Parkinson's Disease and Movement Disorders Unit of the Neurology Service of Hospital Clinic, Carrer de Villarroel 170, 08036 Barcelona, Catalonia, Spain.
E-mail addresses: hbaggio@ub.edu (H.C. Baggio), alexandraabos@ub.edu (A. Abos), bsegura@ub.edu (B. Segura), anna.campabadal@ub.edu (A. Campabadal), carme.uribe@ub.edu (C. Uribe), APEREZ3@clinic.cat (A. Perez-Soriano), JEMUNOZ@clinic.cat (E. Muñoz), YCOMPTA@clinic.cat (Y. Compta), cjunque@ub.edu (C. Junque), mjmarti@clinic.cat (M.J. Marti).
[1] HCB and AA contributed equally to the manuscript.

https://doi.org/10.1016/j.nicl.2019.101720
Received 15 November 2018; Received in revised form 3 February 2019; Accepted 12 February 2019
Available online 13 February 2019

approaches to help distinguish between PD and MSA, mainly using structural and diffusion MRI techniques (Ramli et al., 2015; Huppertz et al., 2016). Another technique, resting-state functional magnetic resonance imaging (fMRI), has shown promising results as a tool for the development of imaging biomarkers with predictive power at the single-subject level in neurodegenerative diseases (Khazaee et al., 2016a; Khazaee et al., 2016b; Hojjati et al., 2017; Challis et al., 2015; Abós et al., 2017). Several studies have described resting-state functional connectivity changes in PD (Prodoehl et al., 2014; Sang et al., 2015; Kim et al., 2017; Baggio et al., 2014; Baggio et al., 2015), and a few have found individual-subject predictive capabilities (Rosskopf et al., 2018; Yao et al., 2017). To the best of our knowledge, however, the potential of resting-state fMRI for subject-level distinction between PD and MSA has not been assessed.

The development of imaging biomarkers to help in the differential diagnosis between diseases such PD and MSA can presumably benefit from the available knowledge regarding their respective pathophysiologies. In advanced disease stages, both PD and MSA are associated with extensive and widespread brain degeneration. In their initial phases, however, more specific areas of vulnerability can be identified. In PD, Lewy pathology is described to progress in a caudo-cranial fashion, often starting at the brainstem (Braak et al., 2003), with marked degeneration of the substantia nigra leading to striatal dopaminergic denervation. MSA, on the other hand, is an α-synucleinopathy mainly characterized pathologically by olivopontocerebellar and striatonigral degeneration (Jellinger, 2014; Burn and Jaros, 2001; Ozawa et al., 2004). While MSA patients can present clinically with a predominantly cerebellar or predominantly parkinsonian phenotype, some degree of cerebellar and striatonigral pathology appears to occur in all MSA patients (Ozawa et al., 2004). These observations suggest that the cerebellum may be the region of greatest differential degeneration between PD and MSA. Based on this, our aim in the present study is to describe the existence and anatomical distribution of abnormalities in resting-state functional connectivity between i. the cerebellum and a set of canonical large-scale intrinsic-connectivity brain networks (ICNs), and ii. the cerebellum and different regions of the striatum in MSA and PD patients.

Considering the early and marked involvement of the cerebellum in MSA described above, we hypothesize that patients with this disease will show altered patterns of functional connectivity between the cerebellum and the cerebrum. Since cerebellar degeneration is not a prominent aspect of PD, we further hypothesize that, compared with healthy subjects, MSA patients will have more severe functional connectivity alterations than PD patients. Finally, we hypothesize that the rich information obtained by assessing the connectivity between the cerebellum and different cerebral networks/striatal regions will allow distinguishing MSA from PD patients with high accuracy.

2. Methods

2.1. Participants

For this study, 37 patients with MSA and 70 patients with PD were initially recruited from the Parkinson's Disease and Movement Disorders Unit, Hospital Clínic de Barcelona. Two samples of healthy controls (HC) were also included, one comprising 20 subjects (used to generate unbiased ICN templates through independent component analysis), and another with 42 subjects used in intergroup comparisons. HC were recruited from individuals who volunteered to participate in scientific studies at the Institut de l'Envelliment, Barcelona. Inclusion criteria were the fulfillment of the UK PD Society Brain Bank diagnostic criteria for PD patients and the Gilman criteria for MSA patients (Gilman et al., 2008). Exclusion criteria were: history of significant neurological (other than PD/MSA for patients) or psychiatric diseases; pathological MRI findings in HC or findings suggestive of alternative diagnoses for PD or MSA patients; mean interframe head motion ≥ 0.3 mm translation or 0.3° rotation during the resting-state acquisition.

Eight PD patients and seven MSA patients were excluded for excessive head motion. One MSA patient was excluded for abnormal pathological MRI findings. One healthy control was excluded for WM hyperintensities and two for excessive motion. The final sample included 59 HC (20 used in independent component analysis, 39 used in intergroup analyses), 62 PD patients (average [standard deviation] disease duration = 8.2 years [5.1]), and 30 MSA patients (average [standard deviation] disease duration = 4.5 years [2.7]).

All PD patients and 22 MSA patients were taking antiparkinsonian drugs, consisting of different combinations of levodopa, catechol-*O*-methyl transferase inhibitors, monoamine oxidase inhibitors, dopamine agonists, and amantadine. All assessments were done while patients were under the effect of their usual medication (*on* state). Levodopa equivalent daily dose (LEDD) was calculated as suggested by Tomlinson et al. (Tomlinson et al., 2010) Motor disease progression and severity were evaluated using the Unified Parkinson's Disease Rating Scale (motor section) for PD patients, the Unified Multiple System Atrophy Rating Scale (motor section) for MSA patients, and the Hoehn and Yahr (HY) scale for both groups (Hoehn and Yahr, 1967). Cognitive and depressive (non-motor) symptoms were assessed using the mini-mental state examination (MMSE) and the Beck Depression Inventory-II (BDI). The study was approved by the institutional ethics committee (Clinical Research Ethics Committee of the Hospital Clínic de Barcelona), all subjects provided written informed consent to participate (IRB00003099), and all methods were performed in accordance with the relevant guidelines and regulations.

3. MRI acquisition and preprocessing

Magnetic resonance images were acquired with a 3T Siemens scanner (MAGNETOM Trio, Siemens, Germany) using an eight-channel head coil. The scanning protocol included a resting-state, 10-min-long functional gradient-echo echo-planar imaging sequence (240 T2*-weighted volumes, TR = 2.5 s, TE = 28 ms, flip angle = 80°, slice thickness = 3 mm, FOV = 240 mm, with 3-mm isotropic voxels, in which subjects were instructed to keep their eyes closed, not to think of anything in particular and not to fall asleep); a high-resolution three-dimensional structural T1-weighted MPRAGE sequence acquired sagittally (TR = 2.3 s, TE = 2.98 ms, 240 slices, FOV = 256 mm; 1 mm isotropic voxel); and a T2-weighted axial FLAIR sequence (TR = 9 s, TE = 96 ms).

Basic functional image preprocessing, using AFNI (http://afni.nimh.nih.gov/afni) and FSL (https://www.fmrib.ox.ac.uk/fsl) tools, included: discarding the first five volumes to allow magnetization stabilization, despiking, motion correction, brain extraction, grand-mean scaling, linear detrending, and high-pass filtering (maintaining frequencies above 0.01 Hz).

4. Resting-state fMRI noise correction

To remove the effects of head motion and other non-neural sources of signal variation from the functional data, we used independent component analysis (ICA)-based strategy for Automatic Removal of Motion Artefacts (ICA-AROMA) (Pruim et al., 2015). Briefly, this method performs ICAs using individual resting-state data sets and automatically identifies artifact-related independent components. The time courses corresponding to artifactual components are subsequently "regressed out" of the data sets.

Average white-matter and cerebrospinal fluid signals, as well as the six motion parameters obtained from the motion correction procedure, were also "regressed out" of the functional images to generate the denoised data sets. To generate the corresponding white matter and cerebrospinal fluid (lateral ventricle) masks, structural images were segmented using FreeSurfer (https://surfer.nmr.mgh.harvard.edu/). The

resulting binary masks were then linearly transformed from structural to native functional space using FSL-FLIRT (https://fsl.fmrib.ox.ac.uk/fsl/fslwiki/FLIRT). To prevent these masks from extending to the adjacent gray matter (GM) due to resampling blur during the linear transform, white matter masks were then "eroded" by applying a threshold of 0.9, while ventricular masks were thresholded at 0.3. Denoised data sets were then non-linearly transformed to MNI space at $3 \times 3 \times 3\,mm^3$ voxel size with SPM (http://www.fil.ion.ucl.ac.uk/spm/) and smoothed with a three-dimensional gaussian kernel of 6 mm FWHM.

5. Cerebellar functional connectivity analyses

Subsequent cerebellar functional connectivity analyses consisted of two approaches: a data-driven approach to assess large-scale ICNs, and a seed-based striatal connectivity analysis.

6. Large-scale intrinsic-connectivity networks

In this analysis, we were interested in characterizing a set of canonical ICNs through a data-driven technique, assessing their respective patterns of connectivity with the cerebellum, and testing for differences in cerebellar connectivity between groups. To avoid biasing results, an independent set of healthy controls was used to generate the network templates, as previously suggested (Griffanti et al., 2016). Specifically, resting-state functional MRI data from 20 healthy controls (acquired in the same scanner using the same acquisition parameters and preprocessed with the same pipeline) were fed into a temporal-concatenation spatial ICA with FSL's MELODIC (https://fsl.fmrib.ox.ac.uk/fsl/fslwiki/MELODIC), with a pre-determined dimensionality of 12 independent components. The spatial and power spectral characteristics of the 12 resulting components were inspected (Griffanti et al., 2017) to identify seven well-established neural networks: the default-mode network (DMN), visual network, left and right frontoparietal networks (FPN), sensorimotor network, dorsal attention network (DAN), and salience network.

The 12 independent components, including the seven networks of interest, were then fed into a dual-regression (Filippini et al., 2009). In this procedure, each group component is used as a spatial regressor to extract a subject and component-specific mean time course, describing the temporal dynamics of each component. These time courses are then used as regressors in a voxel-wise linear model against the resting-state sets of subjects included in subsequent analyses, to generate subject-specific spatial maps for each independent component. Whole-brain voxel-wise one-sample *t*-tests using permutation testing (5000 permutations) and TFCE were performed for the seven networks of interest in the HC group using FSL's randomise. Results are shown in Fig. 1. To assess the connectivity patterns of these seven networks in the cerebellum, the one-sample t-test was repeated while restricting the statistical analysis to cerebellar voxels. To this end, a cerebellar mask was created using the MNI Structural Atlas available in FSL. The original 1-mm-voxel mask was resampled to 3-mm voxel size and thresholded to eliminate voxels with values below 10 (to reduce the inclusion of extra-cerebellar areas due to resample blur).

7. Striatal connectivity analysis

In this section, we performed a seed-based striatal-cerebellar connectivity analysis using the Oxford-GSK-Imanova Striatal Connectivity Atlas, available in FSL (https://fsl.fmrib.ox.ac.uk/fsl/fslwiki/Atlases/striatumconn). This atlas divides the striatum (putamen, caudate nucleus, and nucleus accumbens) into three subdivisions – limbic, executive, and sensorimotor – represented by probabilistic maps. The original 1-mm resolution masks were divided into left-hemisphere and right-hemisphere masks and non-linearly transformed from MNI space to native functional space. The corresponding temporal courses were defined as the first eigenvariate of the weighted time series of the voxels included in each mask, extracted from the native-space resting-state data after the first preprocessing steps (despiking, motion correction, grand-mean scaling, linear detrending, and high-pass filtering) but prior to noise correction.

For each cerebellar voxel, a general linear model was then applied in which the dependent variable was defined as that voxel's time series (extracted from the resting-state data after the first preprocessing steps, normalized to MNI space, and smoothed with a Gaussian kernel of 6 mm FWHM). The independent variables were defined as the temporal course of the corresponding striatal subdivision as well as the time series of the ICA-AROMA artifact components, mean white matter time series, and mean lateral-ventricular time series. The strength of functional connectivity was finally defined as the resulting beta coefficient corresponding to the striatal subdivision temporal course, generating a voxel-wise cerebellar connectivity map for each of the six striatal regions (left and right limbic, left and right executive, and left and right sensorimotor).

For both ICN and striatal-connectivity voxel-wise analyses, testing for intergroup differences was done through permutation testing (5000 permutations) and TFCE using randomise. Age, sex, years of education, and head motion (mean interframe rotation) were included as covariates of no-interest in all comparisons. Statistical significance was set at $p \leq 0.05$, corrected for multiple testing using family-wise error (FWE) correction across space. In the main text we only report significant results whose maximum's *p*-value survived additional Holm-Bonferroni correction for multiple testing (Holm, 1979) (corrected $p \leq 0.05$) accounting for the number of comparisons performed. For ICN analysis, 42 comparisons were made (seven networks by six intergroup comparisons); for striatal connectivity analysis, 36 comparisons were performed (six striatal regions by six intergroup comparisons).

8. Classification procedure

Beyond testing for intergroup differences in cerebellar connectivity, we were interested in assessing the usefulness of these connectivity metrics in discriminating between PD and MSA patients using a supervised learning algorithm. In this classification procedure, we used both ICN-cerebellar and striatal-cerebellar connectivity measures as features.

To avoid circularity, the definition of features was done independently of the results of intergroup comparisons. Specifically, one feature was generated for each "seed" ICN and each striatal subregion, at a total of 13 features. Initially, "physiologic" mean cerebellar connectivity masks for each seed region in the HC group was defined through one-sample *t*-tests: significant voxels at FWE-corrected $p \leq 0.05$ were assigned a value of 1, and all other voxels were set to 0. Subsequently, mean connectivity levels were extracted from these masks from the PD and MSA patient samples, producing a single mean connectivity value for each subject and for each seed ICN/region. Fig. 2 illustrates the pipeline followed for ICN feature definition.

For the classification procedure, we used a support vector machine (SVM), a high-dimensional pattern classification algorithm, performed with the SVM function from scikit-learn (http://scikit-learn.org), implemented in Python, using a radial basis function. Different parameters need to be specified when working with SVM. First, a C parameter that determines the tradeoff between a wide margin and the classifier error. And second, a gamma parameter is required, which defines how far the influence of a single training example reaches. To choose the best kernel and C and gamma parameters, the parameters were optimized by cross-validated grid-search over a parameter grid using the GridSearchCV function from scikit-learn. Leave-one-out cross-validation was used to avoid circularity in patient classification. Leave-one-out cross-validation leaves one subject for testing whereas the remaining n-1 subjects are used for training the classification algorithm, with this process repeated once for each subject. This method prevents

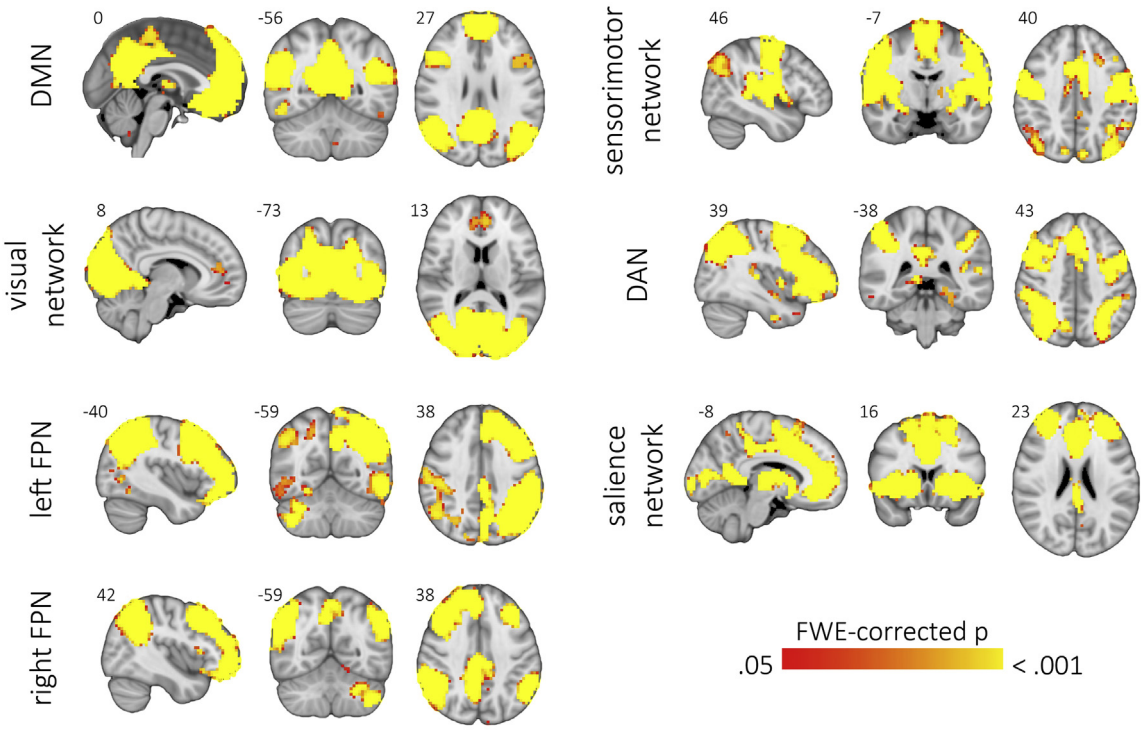

Fig. 1. Large-scale intrinsic connectivity networks of interest.
Images depict the results of the significant (FWE-corrected $p < 0.05$) clusters identified through whole-brain one-sample *t*-tests in the control sample for the seven intrinsic connectivity networks of interest. Individual connectivity maps for each network were obtained through dual regression, performed using spatial maps obtained with independent component analysis performed with an independent control subject sample.

over-fitting, enhances the generalization power of the classifier, and returns an almost unbiased estimate of the probability of test error of the classification (Luntz et al., 1969).

9. Structural gray matter analysis

To assess the concurrent existence and localization of structural gray matter volume abnormalities in PD and MSA patients, we analyzed the structural imaging data using FSL-VBM, an optimized VBM protocol (Douaud et al., 2007). First, structural images were brain-extracted and GM-segmented before being registered to the MNI-152 standard space. The resulting images were averaged to create a study-specific template. Second, native GM images were registered to this template and modulated to correct for local expansion or contraction due to the non-linear component of the spatial transformation. The modulated images were smoothed with an isotropic Gaussian kernel with a sigma of 3 mm. Voxel-wise comparisons were performed with permutation testing (5000 permutations) and TFCE using randomise. Age, sex, and years of education were included as covariates of no-interest. An initial statistical significance threshold was set at $p \leq 0.05$, corrected for multiple comparisons using family-wise error (FWE) correction across space. Results were considered significant if the maximum across voxels of the corresponding contrast survived subsequent Holm-Bonferroni correction accounting for the six comparisons performed.

10. MSA subtype analysis

In the main analyses performed in this study, MSA patients were considered as a single group, regardless of the predominant motor phenotype (cerebellar or parkinsonian). We made this decision because, as with the majority of MSA cases (Wenning et al., 1997), most MSA patients in our study had a mixed phenotype, and due to previous findings indicating that cerebellar degeneration is present even in patients with predominant parkinsonian phenotypes (Ozawa et al., 2004). To assess whether potential intergroup effects in cerebellar connectivity and GM volume were driven by one of the groups, however, we performed additional analyses dividing the MSA group according to clinical phenotype.

Following recommended guidelines (Gilman et al., 2008), patients in our MSA sample were classified as having a cerebellar (MSA-C) or parkinsonian (MSA-P) subtype based on the predominant symptomology. We then performed intergroup comparisons using mean connectivity values from the clusters of significant intergroup cerebellar connectivity differences, the connectivity parameters used as features in the classification procedure, and the mean GM values from the clusters of significant differences between PD and MSA patients. Comparisons were performed using the general linear model, taking age, sex, and education (and mean interframe head motion for connectivity variables) as covariates of no interest. Statistical significance was established through the Monte Carlo method with 10,000 permutations using in-house MATLAB scripts. Statistical significance was set at $p < 0.05$, corrected for multiple testing using the Holm-Bonferroni method. Results, shown as Supplementary data, reveal that both MSA-C and MSA-P had significant connectivity and GM volume reductions compared with both HC and PD patients.

11. Other statistical analyses

Intergroup comparisons involving head motion, sociodemographic data, and functional connectivity variables were performed using the general linear model. Statistical significance was established through the Monte Carlo method with 10,000 permutations using in-house MATLAB scripts. Two-tailed *p*-values were calculated as the proportion of values in the null distribution more extreme than those observed in the actual model. Pearson's chi-squared test was used to compare sex, hand-dominance, and HY score distribution among groups.

Findings were considered significant at an α of 5%, corrected for multiple testing using the Holm-Bonferroni method for the connectivity

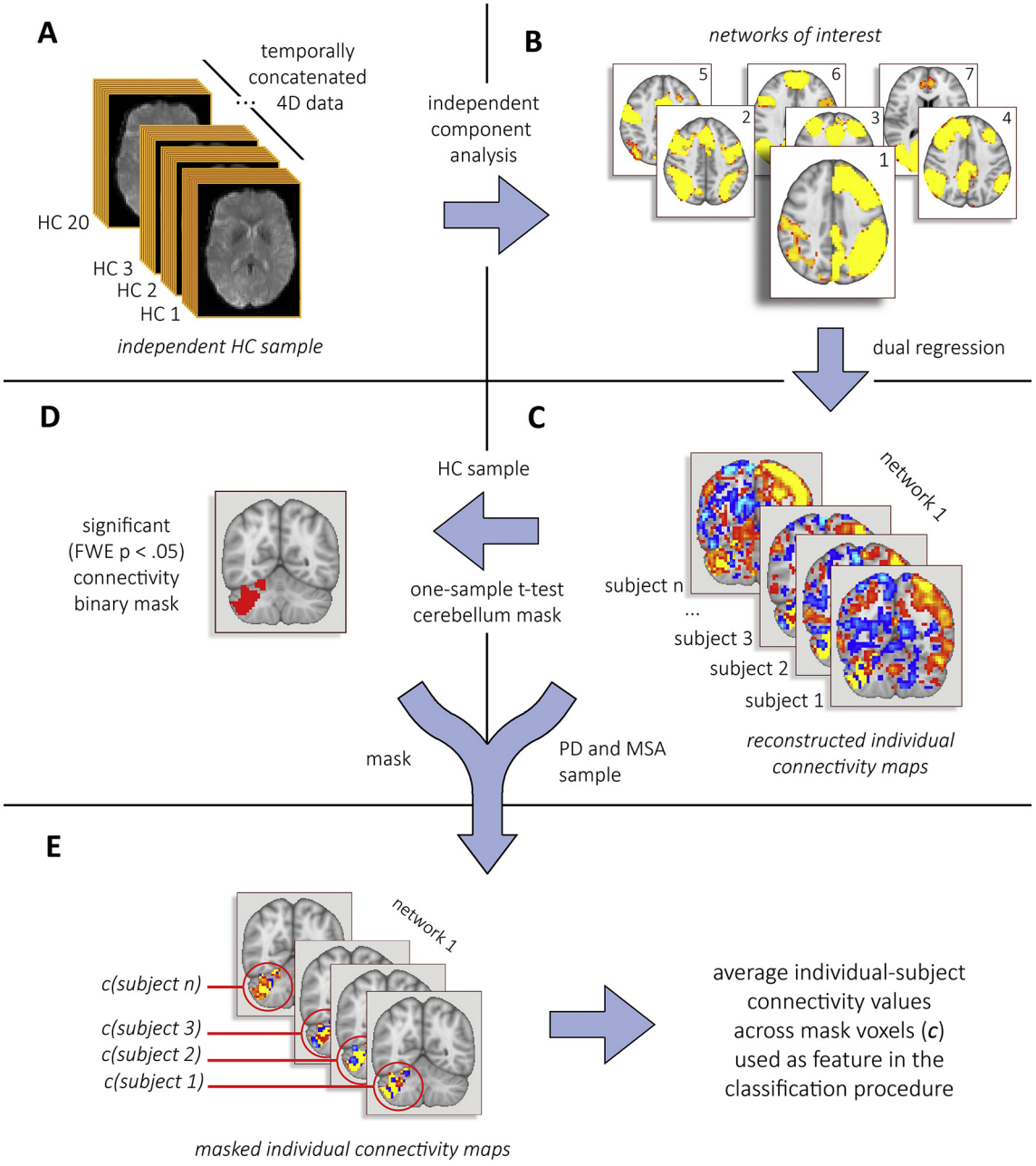

Fig. 2. Schematic representation of the pipeline followed to extract the features used in the classification procedure.
Initially, an independent component analysis was performed using an independent sample of 20 healthy subjects (A). The 12 independent components identified, including the seven networks of interest (default mode, dorsal attention, left and right frontoparietal, salience, sensorimotor, and visual networks) were then fed into a dual regression (B). From the individual network maps reconstructed in dual regression (C), those corresponding to the healthy control (HC) group were then used in a one-sample *t*-test to identify the cerebellar regions of significant connectivity, then used to create one binary mask for each network's "normal" cerebellar connectivity territory (D). Average connectivity levels from the dual regression output were extracted for each subject from each of the seven masks, defining the features used in the classification procedure to distinguish between PD and MSA patients (E).

variables. This correction was made considering seven omnibus comparisons for the ICNs, six omnibus comparisons for the striatal connectivity variables, 21 comparisons for the post-hoc ICN assessment (three two-tailed intergroup comparisons for each of the seven networks), and 18 comparisons for the post-hoc striatal connectivity variables (three two-tailed intergroup tests for each of the six striatal subdivisions).

The relationship between clinical variables and the 13 connectivity values used as features in the classification procedure were assessed separately in the PD (UPDRS and HY scores) and the MSA group (UMSARS and HY scores) also using the general linear model with 10,000 permutations to establish significance. Findings were considered significant at an α of 5%, corrected for multiple testing using the Holm-Bonferroni method.

As an exploratory complementary analysis, we repeated the ICN and striatal voxel-wise group comparisons using a whole-brain mask, to assess whether the hypothesized connectivity differences predominate in the cerebellum (justifying the use of cerebellar connectivity measures as a tool for distinguishing between MSA and PD patients) or whether the cerebellum is a less central component of a more generalized effect. Results that displayed peak FWE-corrected $p \leq 0.01$ are shown in the Supplementary data.

Table 1
Sociodemographic, clinical, and head motion parameters by group.

	HC (n = 39)	PD (n = 62)	MSA (n = 30)	stat/p-value
Age (years)	61.7(11.5)	65.3(10.2)	60.6(8.4)	2.663/.074
Sex (female:male)	22:17	16:46	11:19	9.586χ/.008
Hand dominance (r:l)	38:1	59:3	27:3	1.913χ/.384
Education (years)	13.1(4.2)	12.3(5.5)	10.7(3.8)	2.173/.118
UPDRS	–	16.3(9.3)	–	–
UMSARS	–	–	48.9(20.1)	–
HY (1:2:3:4:5)	-	10:31:20:1:0	0:8:10:9:3	28.631χ/ < .001
LEDD (mg)	-	654.2(376.6)	498.8(432.9)	2.937/.090
Mean rotation (°)	0.037(0.017)	0.049(0.030)	0.047(0.025)	3.011/.053
Mean translation (mm)	0.111(0.061)	0.093(0.052)	0.105(0.062)	1.181/.310

HC: healthy controls; *PD*: Parkinson's disease patient group; *MSA*: multiple system atrophy patient group; *UPDRS*: United Parkinson's Disease Rating Scale, motor section scores; *UMSARS:* United Multiple System Atrophy Rating Scale, motor section scores; *HY:* Hoehn and Yahr scale (number of subjects according to score); *LEDD*: levodopa equivalent daily dose; *Stats* refers to F statistic or Pearson's chi-square (χ).

12. Results

Table 1 shows sociodemographic, clinical, and head motion characteristics for the three groups (HC, PD patients, and MSA patients). Sex distribution was not balanced – men were overrepresented in the PD group – and MSA patients had significantly higher HY scores. Significant intergroup effects were also observed for BDI scores. Post-hoc testing showed that MSA patients had significantly higher BDI scores than both HC and PD patients (both uncorrected $p < .001$), with no significant differences between PD patients and HC (uncorrected $p = .201$). Regarding the MMSE, post-hoc testing showed lower scores in the MSA group compared with HC (uncorrected $p = .015$), with no significant effects between PD and MSA patients (uncorrected $p = .200$) or between PD patients and HC (uncorrected $p = .125$).

13. Cerebellar functional connectivity analyses – intrinsic-connectivity networks

Fig. 1 shows the results of the whole-brain one-sample *t*-test regarding the seven networks of interest in the control group, revealing the typical spatial distribution of this set of canonical ICNs (Smith et al., 2009; Spreng et al., 2013; Thomas Yeo et al., 2011). Fig. 3 depicts these networks' pattern of connectivity when restricting the one-sample t-test to cerebellar voxels in the HC group. Results of one-sample *t*-tests in the three study groups are shown in Supplementary Figs. 1a and b. The patterns of significant cerebellar connectivity for each network in the control group are described below:

- *DMN:* significant co-activation in lobule IX and adjacent vermis, as well as in crus I and crus II bilaterally (with a slight left-hemispheric predominance);
- *Visual network:* co-activation in lobule IX and adjacent vermis, and in lobules VIIb/VIIa bilaterally. Significant co-activation in regions adjacent to the occipital lobe was also seen, probably related to signal "contamination" from the visual cortex;
- *Left FPN:* right-hemispheric co-activation, mainly in crus I and II, with extension to lobules VI and VIIb;
- *Right FPN:* left-hemispheric co-activation, mainly in crus I and II, extending to lobules VI and VIIb;
- *Sensorimotor network:* bilateral symmetrical co-activation of lobules VI and V and adjacent vermis;
- *DAN:* left-hemispheric predominance, involving the posterior parts of crus I, crus II, lobule VI, and lobule VIIb. In the right hemisphere, predominant co-activation in the posterior parts of crus II extending to crus I and lobule VI. Smaller clusters of significant co-activation were also seen in lobule IX and adjacent vermis;
- *Salience network:* bilateral and symmetrical co-activation in the lateral parts of the cerebellar hemispheres, mainly in crus I and crus II, with extension to lobule VI and, in the left hemisphere, lobules VIIb and VIIIa.

Voxel-wise intergroup comparisons revealed that, compared with patients with PD, MSA patients were found to have reduced connectivity between the cerebellum and:

- the left FPN, located in the right crus I/II, extending cranially to lobule VI and caudally to lobule VIIb;
- the sensorimotor network, in lobules V and VI, extending anteriorly to lobule IV bilaterally;
- the salience network, in the left lobule VI and crus I, and in the right crus I and lobules IV and VI;
- the right FPN, in a small region of the left crus I.

These connectivity reductions were mainly located in the regions of stronger connectivity between the cerebellum and the corresponding ICNs described above, as shown in Fig. 3. Except for the one involving the right FPN, all comparisons survived Holm-Bonferroni correction and are depicted in Fig. 4. Significant clusters are described in Table 2.

Compared with HC, MSA patients had reduced cerebellar connectivity with the sensorimotor network and the salience network (FWE-corrected $p \leq .05$). Neither of these comparisons, however, survived subsequent Holm-Bonferroni correction. Results of comparisons that did not survive Holm-Bonferroni correction are shown in Supplementary Fig. 2.

Supplementary whole-brain analyses (Supplementary Fig. 3) showed similar patterns of connectivity reduction in MSA compared with PD patients between the cerebellum and the left FPN, sensorimotor network, and salience network. Regarding the sensorimotor network, a small cluster of reduced connectivity in the subcallosal cortex was also observed.

13.1. Cerebellar functional connectivity analyses – striatal connectivity

Fig. 5 depicts the patterns of resting-state functional connectivity between the six bilateral striatal subregions and the cerebellum in the control group as revealed by one-sample *t*-tests. Supplementary Figs. 4a through c additionally show the results of one-sample *t*-tests in the patient groups. For all striatal subdivisions, extended areas of significant connectivity were observed in HC and PD patients, especially for the executive subregions. Overall, the posterior and lateral portions of crus I and crus II appear to be less connected to the striatum. MSA patients, on the other hand, showed less widespread connectivity, as confirmed by subsequent intergroup testing (see Fig. 6 and Table 3):

Regarding the left sensorimotor striatum, connectivity in MSA patients was significantly reduced compared both with controls and with PD patients. Compared with HC, reduced connectivity in MSA patients was seen in regions of the lobule VI/crus I (especially on the left side) and regions of the lobule IX and VIIIb (mainly on the right side) and

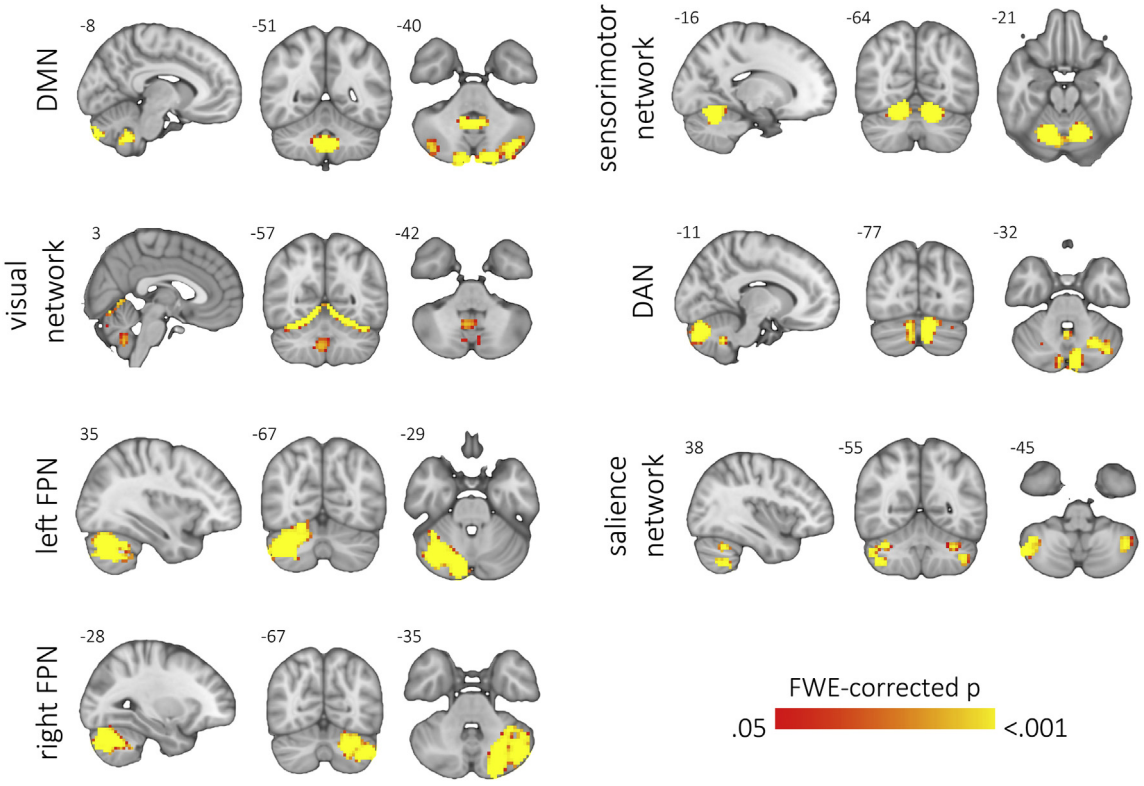

Fig. 3. Large-scale intrinsic-connectivity brain networks – patterns of cerebellar connectivity.
Plots show the results of one-sample *t*-tests for the seven networks of interest, including cerebellar voxels only, performed in the control group. Colored regions represent voxels with values significantly greater than zero (familywise error (FWE)-corrected $p \leq .05$). MNI coordinates (x, y, or z) are shown next to the corresponding slices. In coronal and axial views, the right hemisphere is shown on the left side. *DMN*: default mode network; *FPN*: frontoparietal network; *DAN*: dorsal attention network.

adjacent vermis. A similar but more extended pattern was observed in MSA compared with PD patients, extending to the crus II bilaterally, to the right lobule V, and to lobules VIII and X in the left hemisphere. These comparisons survived Holm-Bonferroni correction.

MSA patients also displayed significantly reduced connectivity between the left executive striatum and the cerebellum, both compared with controls and with PD patients, surviving Holm-Bonferroni correction. Compared with controls, extended areas of connectivity reductions involved lobules VI, VIIb, and VIIIa as well as crus I and II bilaterally. A similar but more extended pattern of connectivity reduction was observed in MSA compared with PD patients, also involving lobules I–IV bilaterally.

Connectivity between the cerebellum and the right executive striatum was also found to be reduced in MSA patients compared both with HC and with PD patients. Only the latter comparison, however, survived Holm-Bonferroni correction. The connectivity reduction in MSA compared with PD patients had a similar pattern to that observed for the left executive striatum.

Regarding the right sensorimotor and right limbic parts of the striatum, MSA patients displayed reduced connectivity compared with PD patients, but these comparisons did not survive Holm-Bonferroni correction. Comparisons that did not survive Holm-Bonferroni correction are shown in the Supplementary data (Supplementary Fig. 5). Supplementary whole-brain analyses (Supplementary Fig. 3) show increased connectivity between the right sensorimotor striatum and extended portions of the cerebral cortex in MSA compared with PD patients.

13.2. Classification procedure results

In this procedure, we used average connectivity values from 13 seed brain networks or striatal regions (seven ICNs defined through ICA and six bilateral striatal subdivisions) to "predict" whether patients belonged to the PD or the MSA patient group. These connectivity values were extracted from the cerebellar regions that were significantly connected to the seeds in the control group, as illustrated in Fig. 2 for the ICNs.

Figs. 7 and 8 display the distribution of the 13 variables used in the classification procedure, including the results of intergroup testing performed on these average values. These variables were then entered as features in a support vector machine, as described in the Methods section. The initial classification was performed using the whole sample of 62 PD patients and 30 MSA patients. This achieved an overall accuracy of 77.17%. Sensitivity (percentage of MSA patients correctly identified) was 83.33% and specificity (percentage of PD patients correctly classified) was 74.19%.

Considering the imbalanced group sizes and the significant differences in sex distribution in the overall sample, we repeated the classification algorithm using a random subsample of PD patients with equal sample sizes ($n = 30$ in both groups) and no significant differences in sex distribution, age, years of education, hand dominance, or head motion parameters. The characteristics of this subsample are given in Supplementary Table 1, and the corresponding distribution of the 13 features used in the classification procedure is shown in Supplementary Figs. 6 and 7. Using these balanced groups, the classification algorithm displayed an overall accuracy of 78.33%, with 80.00% sensitivity and 76.77% specificity.

13.3. Association between clinical and connectivity variables

In this step, we assessed the relationship between the six striatal and seven ICN variables used in the classification procedure and 1.

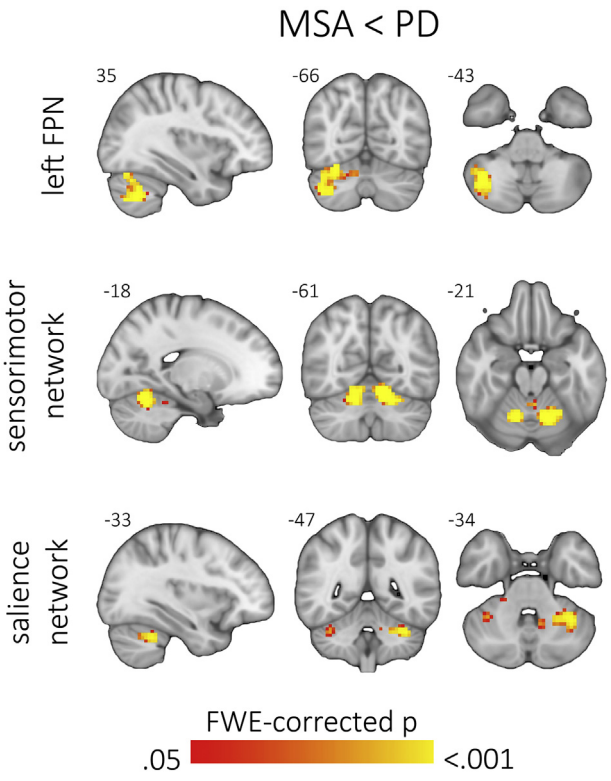

Fig. 4. Intrinsic-connectivity brain networks – cerebellar connectivity intergroup comparisons.
Colored regions depict voxels that displayed significant intergroup effects (familywise error (FWE)-corrected $p \leq .05$, surviving subsequent Holm-Bonferroni correction). *FPN*: frontoparietal network; *MSA*: multiple system atrophy patients; *PD*: Parkinson's disease patients. MNI coordinates (x, y, or z) are shown next to the corresponding slices. In coronal and axial views, the right hemisphere is shown on the left side.

Table 2
Clusters of significant intergroup differences in connectivity between intrinsic connectivity brain networks and the cerebellum.

Contrast	Network	Volume (mm^3)	MNI coordinates of maximum (x,y,z)	FWE-corrected p-value (maximum)
MSA < PD	Left FPN	4185	42, −57, −45	< .001
	SMN	3780	−12, −60, −21	< .001
	Salience network	1089	−36, −51, −33	.001
		162	36, −48, −33	.016
		108	21, −33, −33	.031

MSA: multiple system atrophy patient group; *PD*: Parkinson's disease patient group; *FPN*: frontoparietal network; *SMN*: sensorimotor network.

measures of clinical severity for the PD (UPDRS and HY scores) and the MSA (UMSARS and HY scores) group, and 2. measures of non-motor disease severity (MMSE and BDI). No significant effects were observed for UPDRS or UMSARS scores. For HY scores, a significant effect was observed in the PD group for the average cerebellar connectivity value in the region of significant connectivity with the left executive striatum (Spearman's rho = −.23, uncorrected $p = .016$), not surviving correction for multiple comparisons. No significant effects were observed for the non-motor scales (all uncorrected $p > .05$).

13.4. Structural gray matter analysis

Intergroup VBM analyses revealed significant GM volume reductions in both MSA and PD patients compared with HC, and in MSA patients compared with PD. Reductions in MSA patients compared with HC were observed in extensive areas of the cerebrum, including the prefrontal cortex, precentral gyri, insulae, the striata, the anterior cingulate cortex, lateral and medial temporo-occipital cortex, superior temporal lobules, angular gyri, and basal temporal regions (see Fig. 9). The most statistically significant differences, however, were observed in the cerebellum; extensive effects were observed in the vermis and cerebellar hemispheres bilaterally, mainly sparing lobules I−V and the lateral and posterior portions of crus I and crus II.

GM volume reductions in MSA compared with PD patients were only observed in the cerebellum, where they followed a similar topographical distribution to that found between MSA patients and HC, although somewhat less extensive. Significant volume reductions were also observed in PD patients compared with HC, namely in the orbitofrontal cortex, temporal pole, and inferior lateral occipital cortex bilaterally, left supramarginal gyrus, right anterior insula, and in a small cluster in the right cerebellar hemisphere (lobules VIIb, VIIIa, and VIIIb).

Correlation analyses between average cerebellar GM volumes and the features used in classification, performed separately in the three study groups and taking age into account, showed a correlation with visual network connectivity ($r = .485$, uncorrected $p = .008$) and the right FPN ($r = .398$, uncorrected $p = .032$) in the MSA group. These correlations did not survive Holm-Bonferroni correction for multiple comparisons.

14. Discussion

In the present study, we investigated the existence of alterations in resting-state functional connectivity between the cerebellum and a set of large-scale brain networks, and between the cerebellum and the striatum, in MSA and PD patients. Our results show that MSA patients have reduced functional connectivity between the cerebellum and brain networks such as the left FPN, the sensorimotor network, and the salience network, as well as between the cerebellum and the striatum, predominantly the executive and sensorimotor striatal subdivisions. More importantly, we found evidence that measures of ICN-cerebellar and striatal-cerebellar resting-state functional connectivity can be used to differentiate between PD and MSA patients.

Our first findings – reduced cerebellar functional connectivity in MSA patients – refer to the connectivity between the cerebellum and cortical/subcortical ICNs, and between the cerebellum and different striatal subregions. The cerebellum and the basal ganglia are subcortical structures involved in motor, cognitive, and emotion functions (Strick et al., 2009; Kotz et al., 2009; Middleton and Strick, 2000). These functions are mediated by the dense connections between the cerebellum and the cerebral cortex, as well as between the basal ganglia and the cerebral cortex, forming well-established loops that include the thalamus as an intermediary structure (Percheron et al., 1996; Hoshi et al., 2005). These loops were long thought to be largely independent of each other, interacting essentially via their overlapping cortical territories (Middleton and Strick, 2000). However, extensive disynaptic connections from the basal ganglia to the dentate nucleus (mediated by the thalamus) (Hoshi et al., 2005) and from the cerebellum to the basal ganglia (mediated by pontine nuclei) (Bostan et al., 2010) have been shown to exist in non-human primates. In humans, in vivo evidence of direct connections between the subthalamic nucleus and the cerebellar cortex as well as between the dentate nucleus and the internal globus pallidus has been found using diffusion MRI tractography (Milardi et al., 2016). These findings, taken together with the known vulnerability of the cerebellum and the striatum in MSA, prompted our hypothesis that MSA patients would have connectivity alterations between the cerebellum and brain networks/striatal subregions, confirmed by our results.

Regarding ICNs, we found significantly reduced connectivity between the cerebellum and the left FPN, the sensorimotor network, and the salience network in MSA compared with PD patients. These

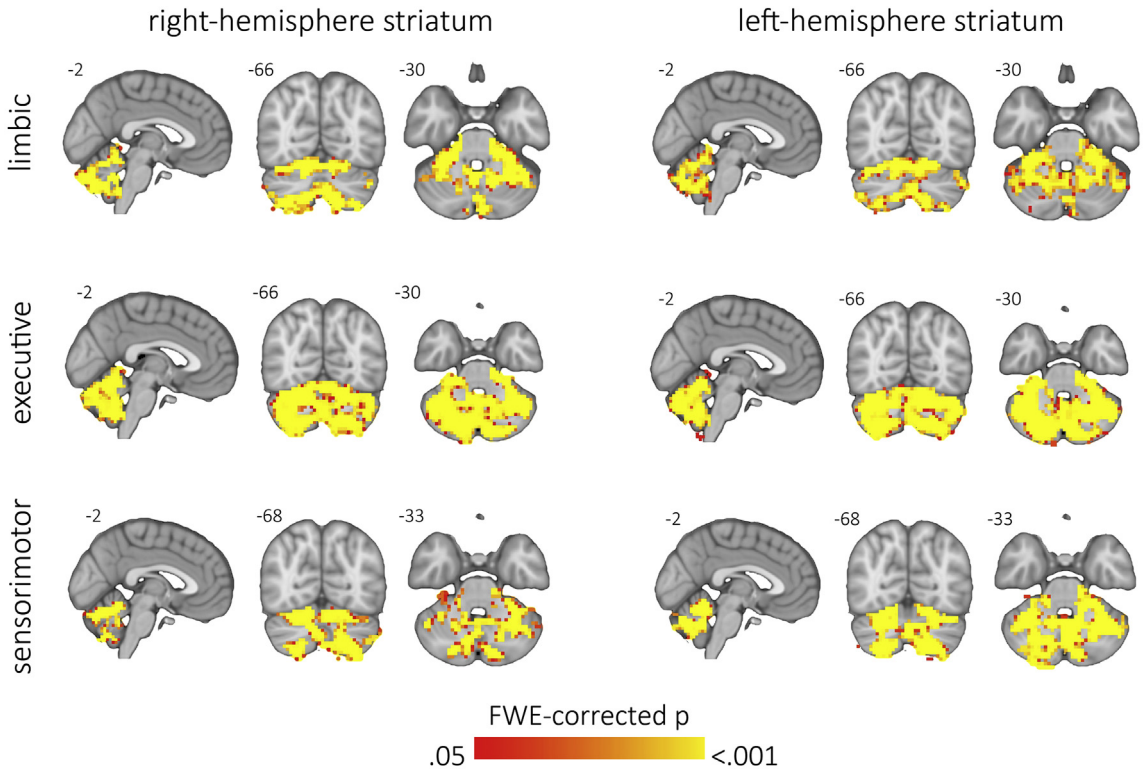

Fig. 5. Striatal subregions – patterns of cerebellar connectivity in the healthy control group.
Images show the results of one-sample t-tests including cerebellar voxels only, performed in the control group, for the right and left limbic (top row), executive (mid row), and sensorimotor (bottom row) striatal subregions. Colored regions represent voxels with values significantly greater than zero (thresholded at familywise error (FWE)-corrected $p \leq .01$). MNI coordinates (x, y, or z) are shown next to the corresponding slices. In coronal and axial views, the right hemisphere is shown on the left side.

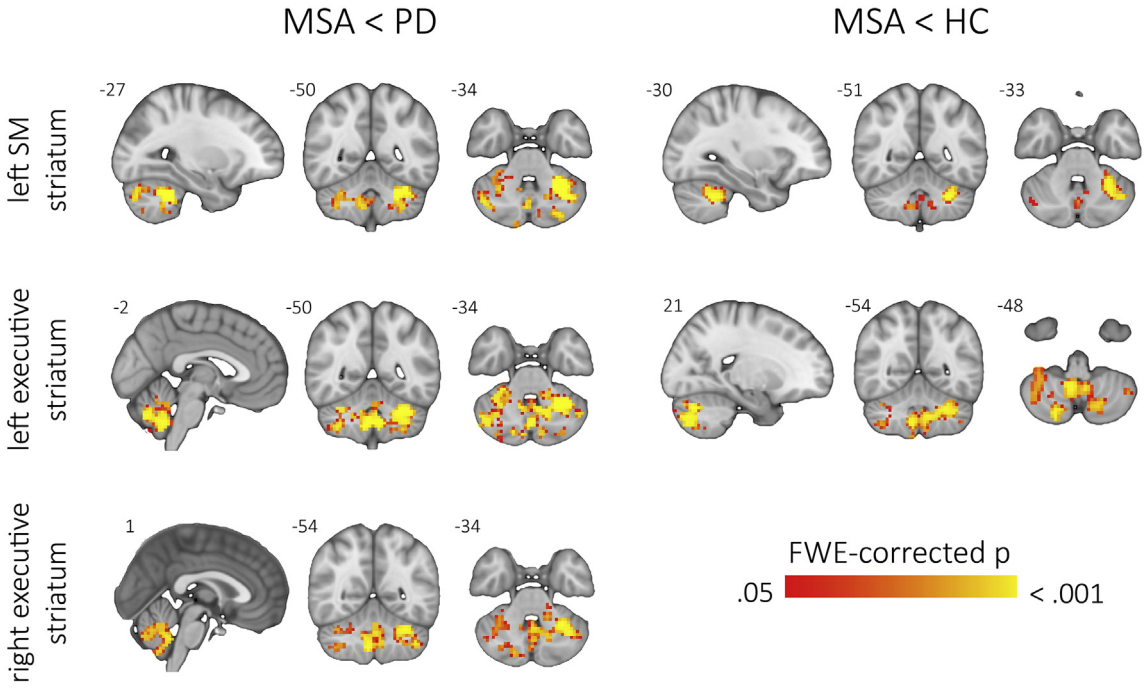

Fig. 6. Striatal subregions – cerebellar connectivity intergroup comparisons.
Colored regions depict voxels that displayed significant intergroup effects (familywise error (FWE)-corrected $p \leq .05$, surviving subsequent Holm-Bonferroni correction). *SM*: sensorimotor; *MSA*: multiple system atrophy patients; *PD*: Parkinson's disease patients; *HC*: healthy controls. MNI coordinates (x, y, or z) are shown next to the corresponding slices. In coronal and axial views, the right hemisphere is shown on the left side.

Table 3
Clusters of significant intergroup differences in connectivity between striatal regions and the cerebellum.

Contrast	Striatal region	Volume (mm3)	MNI coordinates of maximum (x,y,z)	FWE-corrected p-value (maximum)
MSA < HC	Left sensorimotor	5562	−27, −51, −36	< .001
	Left executive	11,547	30, −72, −30	.001
MSA < PD	Left sensorimotor	11,493	−27, −48, −36	.001
	Left executive	16,317	−27, −51, −36	.001
	Right executive	9414	−42, −60, −45	.001

HC: healthy controls; *MSA*: multiple system atrophy patient group; *PD*: Parkinson's disease patient group.

connectivity abnormalities varied in location according to the ICN, tending to occur in areas where the "physiologic" connectivity between the cerebellum and the corresponding network is highest. A similar pattern of connectivity reduction in MSA patients compared with the HC group was observed for the sensorimotor network and the salience network, despite not surviving the final Holm-Bonferroni correction. Regarding striatal connectivity analysis, MSA patients were again found to have reduced cerebellar connectivity compared with PD patients (involving left and right executive and left sensorimotor striatal regions) as well as compared with HC (involving the left executive and sensorimotor striatal regions). Again, differences between MSA and PD patients showed similar anatomical locations but higher significance and greater extension than those between MSA patients and HC. Additional whole-brain connectivity and VBM analyses revealed that the structural and functional abnormalities present between MSA and PD patients are indeed mainly restricted to the cerebellum.

No significant differences were found between PD patients and HC in either ICN or striatal connectivity analyses. While some studies have found altered striatal connectivity in PD, a normalizing effect of dopaminergic replacement therapy has also been described (Szewczyk-Krolikowski et al., 2014; Bell et al., 2015). Our negative results may therefore be related to the fact that patients were scanned in the *on* state. Regarding ICN connectivity, these findings agree with a previous study by our group using a similar approach (Baggio et al., 2015); in this study, significant connectivity abnormalities were not detected when comparing HC and PD patients, and were only observed when

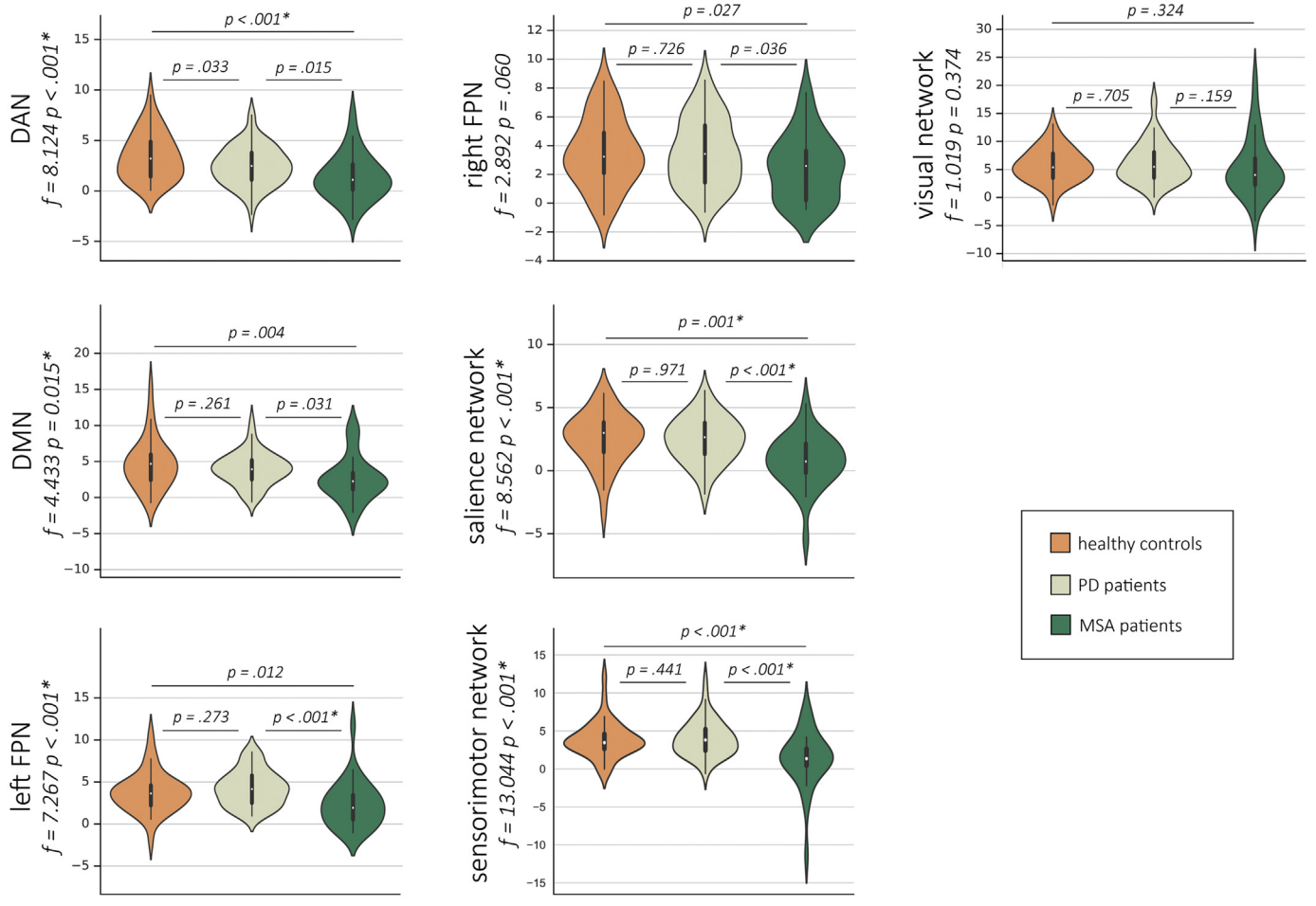

Fig. 7. Parameters of connectivity between intrinsic-connectivity networks and the cerebellum used in the whole-sample classification procedure between PD and MSA patients.
Plots illustrate the distribution of the measures of average connectivity between the cerebellum and the seven intrinsic-connectivity brain networks of interest, used as features in the classification procedure including 30 MSA patients and 62 PD patients. F-statistics and significance of intergroup analyses are shown. Results significant at $p \leq 0.05$, surviving Holm-Bonferroni correction, are marked with an asterisk. *DAN*: dorsal attention network; *DMN*: default mode network; *FPN*: frontoparietal network; *PD*: Parkinson's disease group; *MSA*: multiple system atrophy group.

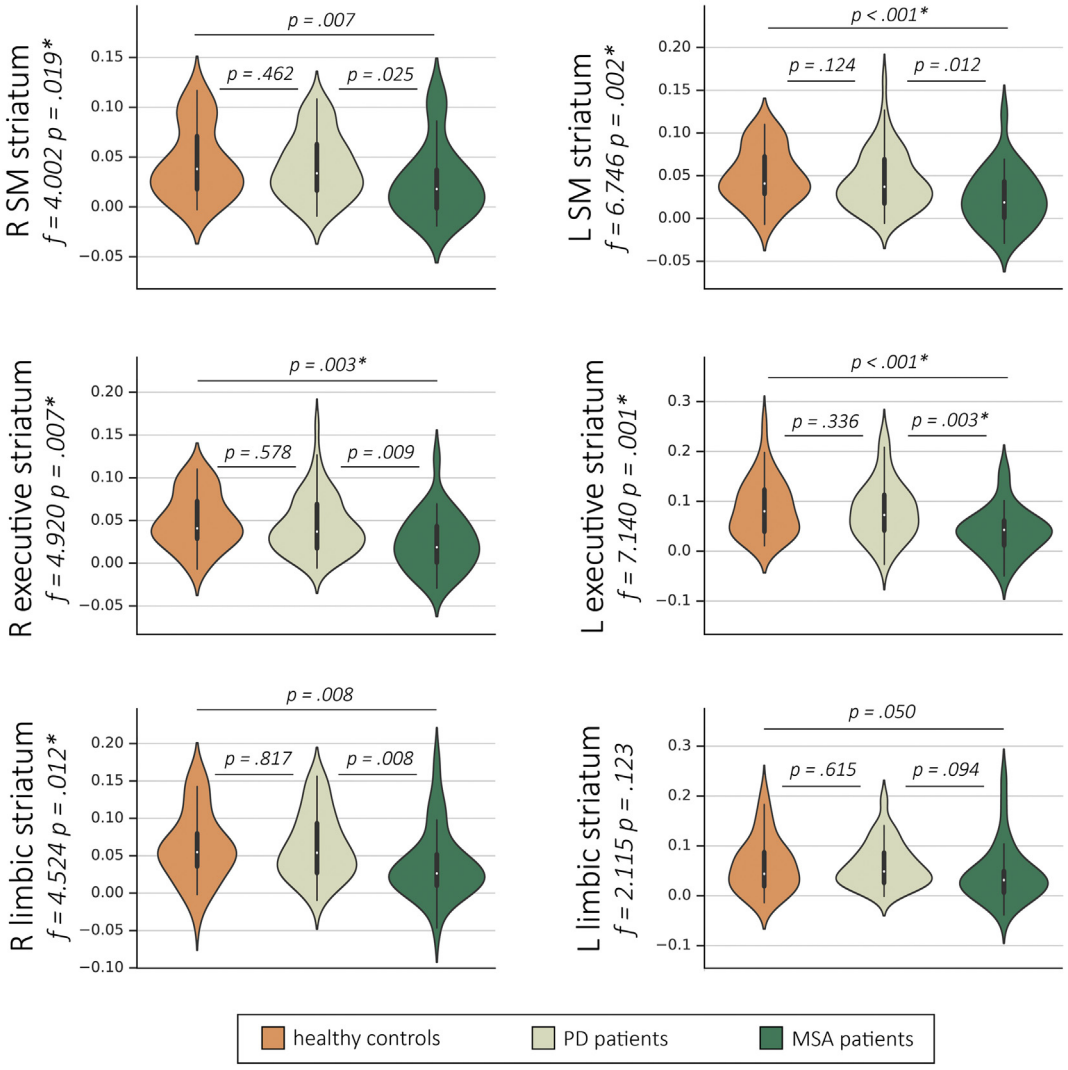

Fig. 8. Parameters of connectivity between striatal subregions and the cerebellum used in the whole-sample classification procedure between PD and MSA patients. Plots illustrate the distribution of the measures of average connectivity between the cerebellum and the six striatal subregions, used as features in the classification procedure including 30 MSA patients and 62 PD patients. F-statistics and significance of intergroup analyses are shown. Results significant at $p \leq 0.05$, surviving Holm-Bonferroni correction, are marked with an asterisk. *R*: right; *L*: left; *SM*: sensorimotor; *PD*: Parkinson's disease group; *MSA*: multiple system atrophy group.

dividing the PD sample according to the presence of cognitive impairment.

Previous findings regarding resting-state cerebellar functional connectivity in MSA are scarce. Yao et al. assessed cerebellar functional connectivity using a seed-based connectivity approach, with the dentate nucleus as the seed region (Yao et al., 2017). These authors found reduced functional connectivity between the left dentate nucleus and the left dorsolateral prefrontal cortex, as well as between the right dentate nucleus and the left precentral gyrus and right dorsolateral prefrontal cortex, in MSA patients compared with controls. In contrast with our study, connectivity was found to be reduced in PD compared with MSA patients, specifically between the left dentate nucleus and the inferior parietal lobe, and between the right dentate nucleus and the posterior cingulate cortex. More recently, Rosskopf et al. found MSA patients to have increased local connectivity in a ponto-cerebellar network compared with controls (Rosskopf et al., 2018). The comparison of these results with the current study, however, are hindered by the different seed and target definition used in connectivity analyses, as well as very different image preprocessing strategies.

While the motor repercussions of cerebellar dysfunction are well known, evidence for non-motor clinical consequences in patients is sparse (Miall, 2016). Recent studies, however, indicate that anterior lobe lesions are associated with the cerebellar motor syndrome of gait ataxia and limb dysmetria; posterior lobe damage, on the other hand, would lead to cognitive/affective manifestations (Schmahmann, 2019; Stoodley et al., 2016). These findings agree with the observed patterns of ICN cerebellar connectivity seen in the present study: networks typically associated with cognitive processing (DMN, DAN, FPNs, and salience network) showed strongest connectivity with posterior lobe regions, especially crus I/II. The sensorimotor network, on the other hand, was mainly connected with more anterior regions, mainly lobules V/VI. We might surmise that the cerebellar connectivity abnormalities observed for a given network underlie deficits in functions subserved by that network – either motor or cognitive. Regarding striatal connectivity, reductions were mostly observed in the posterior lobes, but also extended to anterior regions. As such, these abnormalities might be related to both motor and non-motor aspects of MSA. Since we found no significant correlations between cognitive/motor severity scales and connectivity parameters, however, this remains speculative.

Cerebellar abnormalities also occur in PD (Wu and Hallett, 2013). The existence of connections linking cortico-striatal and cortico-cerebellar loops, described above, provides a potential anatomical basis for this relationship (Wu and Hallett, 2013). Because the cerebellum is not among the most vulnerable brain regions in the degenerative process in

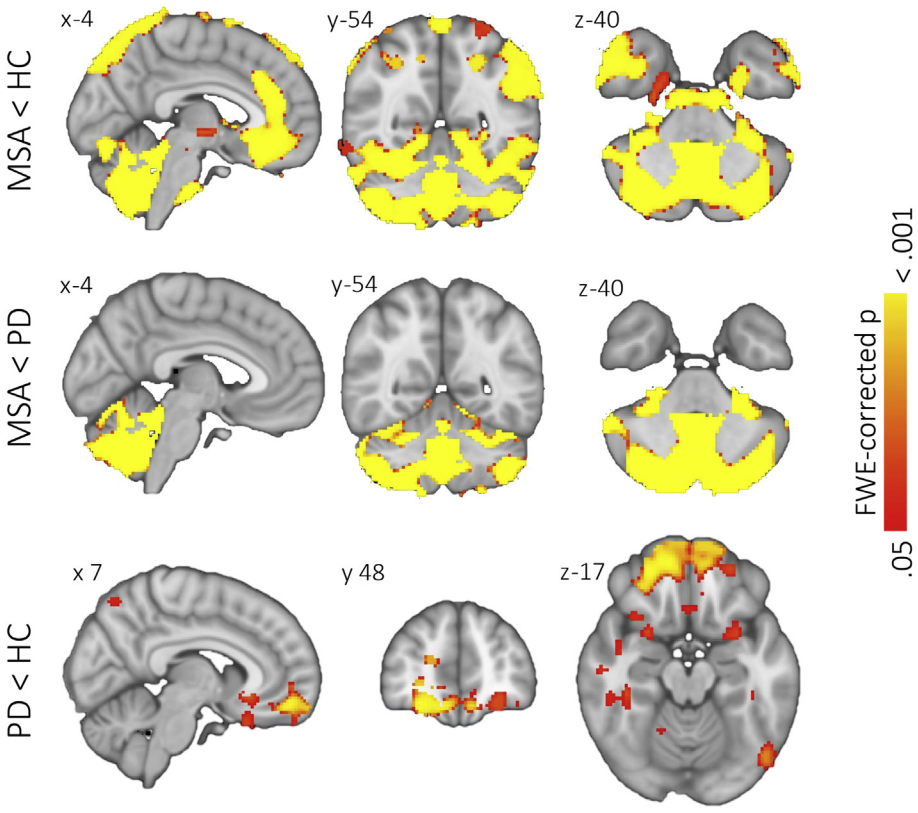

Fig. 9. Voxel-based morphometry – intergroup comparisons.
Images show the regions of significant intergroup differences in gray matter volume ($p < .05$, FWE-corrected, surviving subsequent Holm-Bonferroni correction). HC: healthy controls; MSA: multiple system atrophy patients; PD: Parkinson's disease patients. MNI coordinates (x, y, or z) are shown next to the corresponding slices. In coronal and axial views, the right hemisphere is shown on the left side.

PD, however, we hypothesized that possible connectivity abnormalities seen in our PD sample would on average be less marked than those observed in the MSA group. In fact, we found no significant differences between PD patients and controls for any of the comparisons performed. Previous studies have assessed the resting-state functional connectivity of the cerebellum in PD, with somewhat inconsistent findings. In a recent study, Hou et al., assessing drug-naïve PD patients, found increased connectivity between the cerebellum and both the paracentral lobule and sensorimotor areas (Hou et al., 2018). In a study assessing PD patients in both the *on* and *off* states, Wu et al. found increased connectivity between the motor network and the cerebellum in the *off* state, but not the *on* state (Wu et al., 2009). Also using an *on-off* state design, increases in cerebellar functional connectivity in the *off* compared with the *on* state have been observed with the posterior cortex (Ng et al., 2017; Festini et al., 2015) and with the putamen (Simioni et al., 2016). Such increases in functional connectivity have been hypothesized to be related to a compensatory effect (Wu and Hallett, 2013; Festini et al., 2015; Simioni et al., 2016). By contrast, Hacker et al. found reductions in the functional connectivity between the striatum and the cerebellum in medicated PD patients (Hacker et al., 2012). Assessing the correlation between cerebellar structural parameters and functional connectivity between the cerebellum and ICNs in PD, O'Callaghan et al. found that cerebellar atrophy can lead to both increases and decreases in connectivity (O'Callaghan et al., 2016). These findings indicate that measures of cerebellar connectivity in PD may vary according to factors such as medication status and degree of structural degeneration, and possibly also to technical aspects related to the analytic approach used.

In the second part of our analyses, we found that parameters of resting-state functional connectivity between ICNs and the cerebellum combined with parameters of connectivity between the striatum and the cerebellum allow differentiating between PD and MSA patients with a high overall accuracy and high sensitivity in both groups. This high accuracy was observed both when using the whole patient sample and when using the subsamples with equal numbers of subjects and more similar sociodemographic characteristics. Previous studies have used different MRI-derived measures and machine-learning approaches to assess the potential of neuroimaging in individual-level classification. Resting-state functional connectivity parameters have shown high accuracy in discriminating between healthy controls, patients with mild cognitive impairment, and Alzheimer's disease patients (Challis et al., 2015; Khazaee et al., 2016c; Khazaee et al., 2015), between PD patients with and without cognitive impairment (Abós et al., 2017; Kawabata et al., 2018), between PD patients and healthy subjects (Chen et al., 2015), and between PD patients with and without dyskinesias (Herz et al., 2016). Other studies have used MRI techniques, such as structural MRI (Huppertz et al., 2016), diffusion-weighted imaging (Planetta et al., 2016), or a multimodal imaging data (Péran et al., 2018; Du et al., 2017), as input in machine-learning algorithms to distinguish between MSA and PD patients; to our knowledge, however, this is the first study to use resting-state functional connectivity data to this end. Our findings suggest that measures of functional connectivity between the cerebellum and both the striatum and large-scale brain networks may also be useful in distinguishing PD from MSA patients.

To avoid circularity, the definition of the ICN and striatal subregion features used in the classification algorithm was entirely independent of the intergroup results obtained in the first part of the study. Specifically, the connectivity parameters were extracted from the cerebellar regions that were connected (as defined by regression coefficients significantly > 0) to each ICN or striatal region in the control group. The regions of highest connectivity between the cerebellum and the brain networks of interest found in the present study (shown in Fig. 3) are consistent with those described in previous reports (Habas et al., 2009; Dobromyslin et al., 2012). This suggests that our findings are not idiosyncratic of our data set and that the cerebellar components of the ICNs studied are, like their cerebral counterparts, highly consistent and reproducible. Assuring this consistency is critical for extrapolating our approach to further studies or to the clinical practice. Regarding the normal patterns of functional connectivity of different striatal subregions, we observed extensive areas of significant

connectivity with the cerebellum, especially for the executive striatal subregion. As we found no previous studies that provide information that can be directly compared with our findings, the generalizability of the striatal connectivity patterns observed here should be assessed in future studies.

Some limitations to the present study should be pointed out. The first limitation refers to the fact that our patient samples were not in the early stages of the diseases addressed. To have diagnostic usefulness as imaging markers, the connectivity parameters used here must also display good discrimination ability in early PD and MSA. Therefore, the approach used in the current work should be tested in future studies with newly-diagnosed patients. This includes scanning patients in the *off* state to remove the potentially normalizing effects of dopaminergic replacement therapy. Since cerebellar pathology occurs early in the course of MSA, we expect this approach to also display discriminative power in this setting. Still regarding disease evolution, the MSA patients in our sample had more severe motor disease and more severe depressive symptoms than the PD group despite shorter disease duration. This is not surprising considering that MSA tends to have a more aggressive clinical course, but we cannot rule out that these differences affected the classification procedure. No significant correlations were found between the variables used as features and motor or non-motor scale scores, however, suggesting that the role played by differences in disease severity in the classification procedure was small. The lack of a definitive diagnosis, which could only be obtained through postmortem pathological examination, also means that a few patients are likely to have been misdiagnosed. As another limitation, while we did include a cross-validation procedure to avoid using the test subjects in the model generation, a larger sample would have allowed the use of cross-validation procedures with smaller variance than leave-one-out cross validation. Finally, a common limitation when studying patients with movement disorders is the occurrence of head motion during the resting-state scan, which will inevitably affect the estimated connectivity measures. We have, however, excluded subjects with excessive motion and used a state-of-the-art preprocessing pipeline to reduce the effect of motion artefacts. Additionally, since no differences were observed in head motion parameters between PD and MSA patients, these artefacts are unlikely to have affected the performance of the classification algorithm significantly.

15. Conclusions

In this study we demonstrate the existence of reduced resting-state functional connectivity between the cerebellum and large-scale intrinsic-connectivity brain networks, as well as between the cerebellum and different striatal regions, in patients with MSA compared with healthy subjects as well as compared with PD patients. We also show for the first time that parameters of cerebellar resting-state functional connectivity have the potential to help distinguish between MSA and PD patients at the single-subject level with high accuracy.

Acknowledgments

We are most grateful to the neurologists involved in the Catalan multiple system atrophy registry (CMSAR), the patients, their families, and control subjects for their cooperation. We are also indebted to the Magnetic Resonance Imaging core facility of the IDIBAPS for the technical support; and we would also like to acknowledge the CERCA Programme/Generalitat de Catalunya.

Funding

AA was supported by a 2016 fellowship from the Departament d'Empresa i Coneixement de la Generalitat de Catalunya, AGAUR (2016FI_B 00360), AC was supported by APIF predoctoral fellowship from the University of Barcelona (2017–2018) and CU was supported by a fellowship from 2014, Spanish Ministry of Economy and Competitiveness (BES-2014-068173) and cofinanced by the European Social Fund (ESF). This study was sponsored by the Spanish Ministry of Economy and Competitiveness (PSI2013-41393-P; PSI2017-86930-P cofinanced by Agencia Estatal de Investigación (AEI) and the European Regional Development Fund), by Generalitat de Catalunya (2017SGR748) and by Fundació La Marató de TV3 in Spain (20142310; PI043296). MJM has received funding from Spain's Fondo de Investigaciones Sanitarias (FIS PI17/00096) and from Generalitat de Catalunya (AGAUR 2017SGR1502).

Disclosures

AA, HCB, BS, AC, CU, DM, AP, EM, and CJ report no disclosures. MJM received honoraria for advice and lecture from Abbvie, Bial and Merzt Pharma and grants from Michael J. Fox Foundation for Parkinson Disease (MJFF): MJF_PPMI_10_001, PI044024. YC has received funding in the past five years from FIS/FEDER, H2020 programme, Union Chimique Belge (UCB pharma), Teva, Medtronic, Abbvie, Novartis, Merz, Piramal Imaging, and Esteve, Bial, and Zambon. YC is currently an associate editor for Parkinsonism and Related Disorders.

Conflicts of interest

The authors report no conflicts of interest relevant to this study.

Appendix A. Supplementary data

Supplementary data to this article can be found online at https://doi.org/10.1016/j.nicl.2019.101720.

References

Abós, A., et al., 2017. Discriminating cognitive status in Parkinson's disease through functional connectomics and machine learning. Sci. Rep. 7, 45347.
Baggio, H.-C., et al., 2014. Functional brain networks and cognitive deficits in Parkinson's disease. Hum. Brain Mapp. 35, 4620–4634.
Baggio, H.-C., et al., 2015. Cognitive impairment and resting-state network connectivity in Parkinson's disease. Hum. Brain Mapp. 36, 199–212.
Bell, P.T., et al., 2015. Dopaminergic basis for impairments in functional connectivity across subdivisions of the striatum in Parkinson's disease. Hum. Brain Mapp. 36, 1278–1291.
Bostan, A.C., Dum, R.P., Strick, P.L., 2010. The basal ganglia communicate with the cerebellum. Proc. Natl. Acad. Sci. U. S. A. 107, 8452–8456.
Braak, H., et al., 2003. Staging of brain pathology related to sporadic Parkinson's disease. Neurobiol. Aging 24, 197–211.
Burn, D.J., Jaros, E., 2001. Multiple system atrophy: cellular and molecular pathology. Mol. Pathol. 54, 419–426.
Challis, E., et al., 2015. Gaussian process classification of Alzheimer's disease and mild cognitive impairment from resting-state fMRI. NeuroImage 112, 232–243.
Chen, Y., et al., 2015. Discriminative analysis of Parkinson's disease based on whole-brain functional connectivity. PLoS One 10, e0124153.
Dobromyslin, V.I., et al., 2012. Distinct functional networks within the cerebellum and their relation to cortical systems assessed with independent component analysis. NeuroImage 60, 2073–2085.
Douaud, G., et al., 2007. Anatomically related grey and white matter abnormalities in adolescent-onset schizophrenia. Brain 130, 2375–2386.
Du, G., et al., 2017. Combined diffusion tensor imaging and apparent transverse relaxation rate differentiate Parkinson disease and atypical parkinsonism. Am. J. Neuroradiol. 38, 966–972.
Festini, S.B., et al., 2015. Altered cerebellar connectivity in Parkinson's patients ON and OFF L-DOPA medication. Front. Hum. Neurosci. 9, 214.
Filippini, N., et al., 2009. Distinct patterns of brain activity in young carriers of the APOE-epsilon4 allele. Proc. Natl. Acad. Sci. U. S. A. 106, 7209–7214.
Gilman, S., et al., 2008. Second consensus statement on the diagnosis of multiple system atrophy. Neurology 71, 670–676.
Griffanti, L., et al., 2016. Challenges in the reproducibility of clinical studies with resting state fMRI: an example in early Parkinson's disease. NeuroImage 124, 704–713.
Griffanti, L., et al., 2017. Hand classification of fMRI ICA noise components. NeuroImage 154, 188–205.
Habas, C., et al., 2009. Distinct cerebellar contributions to intrinsic connectivity networks NIH public access. J. Neurosci. 29, 8586–8594.
Hacker, C.D., Perlmutter, J.S., Criswell, S.R., Ances, B.M., Snyder, A.Z., 2012. Resting state functional connectivity of the striatum in Parkinson's disease. Brain 135, 3699–3711.

Herz, D.M., et al., 2016. Resting-state connectivity predicts levodopa-induced dyskinesias in Parkinson's disease. Mov. Disord. 31, 521–529.
Hoehn, M.M., Yahr, M.D., 1967. Parkinsonism: onset, progression and mortality. Neurology 17, 427–442.
Hojjati, S.H., Ebrahimzadeh, A., Khazaee, A., Babajani-Feremi, A., 2017. Alzheimer's Disease Neuroimaging Initiative. Predicting conversion from MCI to AD using resting-state fMRI, graph theoretical approach and SVM. J. Neurosci. Methods 282, 69–80.
Holm, S., 1979. A simple sequentially rejective multiple test procedure. Scand. J. Stat. 6, 65–70.
Hoshi, E., Tremblay, L., Féger, J., Carras, P.L., Strick, P.L., 2005. The cerebellum communicates with the basal ganglia. Nat. Neurosci. 8, 1491–1493.
Hou, Y., et al., 2018. Patterns of striatal and cerebellar functional connectivity in early-stage drug-naïve patients with Parkinson's disease subtypes. Neuroradiology. https://doi.org/10.1007/s00234-018-2101-6.
Hughes, A.J., Ben-Shlomo, Y., Daniel, S.E., Lees, A.J., 1992. What features improve the accuracy of clinical diagnosis in Parkinson's disease: a clinicopathologic study. Neurology 42, 1142–1146.
Hughes, A.J., Daniel, S.E., Ben-Shlomo, Y., Lees, A.J., 2002. The accuracy of diagnosis of parkinsonian syndromes in a specialist movement disorder service. Brain 125, 861–870.
Huppertz, H.-J., et al., 2016. Differentiation of neurodegenerative parkinsonian syndromes by volumetric magnetic resonance imaging analysis and support vector machine classification. Mov. Disord. 31, 1506–1517.
Jellinger, K.A., 2014. Neuropathology of multiple system atrophy: new thoughts about pathogenesis. Mov. Disord. 29, 1720–1741.
Kawabata, K., et al., 2018. Distinct manifestation of cognitive deficits associate with different resting-state network disruptions in non-demented patients with Parkinson's disease. J. Neurol. 265, 688–700.
Khazaee, A., Ebrahimzadeh, A., Babajani-Feremi, A., 2015. Identifying patients with Alzheimer's disease using resting-state fMRI and graph theory. Clin. Neurophysiol. 126, 2132–2141.
Khazaee, A., Ebrahimzadeh, A., Babajani-Feremi, A., 2016a. Application of advanced machine learning methods on resting-state fMRI network for identification of mild cognitive impairment and Alzheimer's disease. Brain Imaging Behav. 10, 799–817.
Khazaee, A., Ebrahimzadeh, A., Babajani-Feremi, A., 2016b. Classification of patients with MCI and AD from healthy controls using directed graph measures of resting-state fMRI. Behav. Brain Res. https://doi.org/10.1016/j.bbr.2016.06.043.
Khazaee, A., Ebrahimzadeh, A., Babajani-Feremi, A., 2016c. Application of advanced machine learning methods on resting-state fMRI network for identification of mild cognitive impairment and Alzheimer's disease. Brain Imaging Behav. 10, 799–817.
Kim, J., et al., 2017. Abnormal intrinsic brain functional network dynamics in Parkinson's disease. Brain 140, 2955–2967.
Koga, S., et al., 2015. When DLB, PD, and PSP Masquerade as MSA an Autopsy Study of 134 Patients.
Kotz, S.A., Schwartze, M., Schmidt-Kassow, M., 2009. Non-motor basal ganglia functions: a review and proposal for a model of sensory predictability in auditory language perception. Cortex 45, 982–990.
Litvan, I., et al., 1998. Accuracy of the clinical diagnoses of Lewy body disease, Parkinson disease, and dementia with Lewy bodies: a clinicopathologic study. Arch. Neurol. 55, 969–978.
Luntz, A., Brailovsky, V., et al., 1969. Techicheskaya Kibern 3.
Miall, R.C., 2016. Neuroscience in the 21st Century 1277–1295. Springer, New York. https://doi.org/10.1007/978-1-4939-3474-4_38.
Middleton, F.A., Strick, P.L., 2000. Basal ganglia and cerebellar loops: motor and cognitive circuits. Brain Res. Brain Res. Rev. 31, 236–250.
Milardi, D., et al., 2016. Extensive direct subcortical cerebellum-basal ganglia connections in human brain as revealed by constrained spherical deconvolution tractography. Front. Neuroanat. 10, 29.
Ng, B., et al., 2017. Distinct alterations in Parkinson's medication-state and disease-state connectivity. NeuroImage Clin. 16, 575–585.
O'Callaghan, C., et al., 2016. Cerebellar atrophy in Parkinson's disease and its implication for network connectivity. Brain 139, 845–855.
Ozawa, T., et al., 2004. The spectrum of pathological involvement of the striatonigral and olivopontocerebellar systems in multiple system atrophy: clinicopathological correlations. Brain 127, 2657–2671.
Péran, P., et al., 2018. MRI supervised and unsupervised classification of Parkinson's disease and multiple system atrophy. Mov. Disord. 33, 600–608.
Percheron, G., François, C., Talbi, B., Yelnik, J., Fénelon, G., 1996. The primate motor thalamus. Brain Res. Brain Res. Rev. 22, 93–181.
Planetta, P.J., et al., 2016. Free-water imaging in Parkinson's disease and atypical parkinsonism. Brain 139, 495–508.
Prodoehl, J., Burciu, R.G., Vaillancourt, D.E., 2014. Resting state functional magnetic resonance imaging in Parkinson's disease. Curr. Neurol. Neurosci. Rep. 14, 448.
Pruim, R.H.R., et al., 2015. ICA-AROMA: a robust ICA-based strategy for removing motion artifacts from fMRI data. NeuroImage 112, 267–277.
Ramli, N.M., Nair, S.R., Ramli, N.M., Lim, S.Y., 2015. Differentiating multiple-system atrophy from Parkinson's disease. Clin. Radiol. 70, 555–564.
Rosskopf, J., et al., 2018. Hyperconnective and hypoconnective cortical and subcortical functional networks in multiple system atrophy. Parkinsonism Relat. Disord. 49, 75–80.
Sang, L., et al., 2015. Alteration of brain functional networks in early-stage Parkinson's disease: a resting-state fMRI study. PLoS One 10, e0141815.
Schmahmann, J.D., 2019. The cerebellum and cognition. Neurosci. Lett. 688, 62–75.
Schrag, A., Ben-Shlomo, Y., Quinn, N., 2002. How valid is the clinical diagnosis of Parkinson's disease in the community? J. Neurol. Neurosurg. Psychiatry 73, 529–534.
Simioni, A.C., Dagher, A., Fellows, L.K., 2016. Compensatory striatal–cerebellar connectivity in mild–moderate Parkinson's disease. NeuroImage Clin. 10, 54–62.
Smith, S.M., et al., 2009. Correspondence of the brain's functional architecture during activation and rest. Proc. Natl. Acad. Sci. U. S. A. 106, 13040–13045.
Spreng, R.N., Sepulcre, J., Turner, G.R., Stevens, W.D., Schacter, D.L., 2013. Intrinsic architecture underlying the relations among the default, dorsal attention, and frontoparietal control networks of the human brain. J. Cogn. Neurosci. 25, 74–86.
Stoodley, C.J., Macmore, J.P., Makris, N., Sherman, J.C., Schmahmann, J.D., 2016. Location of lesion determines motor vs. cognitive consequences in patients with cerebellar stroke. YNICL 12, 765–775.
Strick, P.L., Dum, R.P., Fiez, J.A., 2009. Cerebellum and nonmotor function. Annu. Rev. Neurosci. 32, 413–434.
Szewczyk-Krolikowski, K., et al., 2014. Functional connectivity in the basal ganglia network differentiates PD patients from controls. Neurology 83, 208–214.
Thomas Yeo, B.T., et al., 2011. The organization of the human cerebral cortex estimated by intrinsic functional connectivity. J. Neurophysiol. 106, 1125–1165.
Tomlinson, C.L., et al., 2010. Systematic review of levodopa dose equivalency reporting in Parkinson's disease. Mov. Disord. 25, 2649–2653.
Wenning, G.K., Tison, F., ben Shlomo, Y., Daniel, S.E., Quinn, N.P., 1997. Multiple system atrophy: a review of 203 pathologically proven cases. Mov. Disord. 12, 133–147.
Wu, T., Hallett, M., 2013. The cerebellum in Parkinson's disease. Brain 136, 696–709.
Wu, T., et al., 2009. Changes of functional connectivity of the motor network in the resting state in Parkinson's disease. Neurosci. Lett. 460, 6–10.
Yao, Q., et al., 2017. Altered functional and causal connectivity of cerebello-cortical circuits between multiple system atrophy (Parkinsonian type) and Parkinson's disease. Front. Aging Neurosci. 9, 266.